Supporting Information for

Identifying hydroxylated copper dimers in SSZ-13 via UV-vis-NIR spectroscopy

Florian Göltl[1], Saurabh Bhandari[2], Edgard A. Lebrón-Rodríguez[2], Jake I. Gold[2], Stacey I. Zones[3], Ive Hermans[2,4], James A. Dumesic[2], Manos Mavrikakis[2]

[1] The University of Arizona, Department of Biosystems Engineering, 1177, E 4th St., 85719, Tucson, AZ, United States
[2]The University of Wisconsin – Madison, Department of Chemical and Biological Engineering, 1415 Engineering Drive, 53706 Madison, WI, United States
[3] Chevron Energy Technology Company, Richmond, CA, 94804, United States
[4] The University of Wisconsin – Madison, Department of Chemistry, 1101 University Avenue, 53706 Madison, WI, United States
email: fgoeltl@arizona.edu; emavrikakis@wisc.edu

S1: Methods

S1.1: Computational Methods:

All calculations were carried out using VASP[1], version 5.4.1, a plane wave electronic structure code, where the electron-ion interactions are described within the projector augmented wave method[2,3]. All calculations were carried out sampling only the Γ-point, with an energy cut off of 420 eV. To obtain optical spectra, molecular dynamics simulations for the structures (see structures in Fig. 1 of the main text) were performed using the PBE functional. An Anderson-thermostat with a collision probability of 0.015 for each atom and a time step of 1 fs was used to keep the system at 300 K. After equilibration for 1 ps, optical spectra were calculated every 100 ps for a total of 420 snapshots obtained from a molecular dynamics simulation, each separated by 100 ps, which lead to a total sampling time of 42 ps. It has been shown that optical spectra are well converged using this approach[4]. In the calculation of optical spectra, the number of occupied and empty bands was set to a total of 3040. In a first step, the wave functions were optimized using a HSE-type functional with the exact exchange increased to 40%. To determine the optical properties, the time dependent Casida equation[5] was solved with the amount of exact exchange chosen to be 0.4. This value was chosen to accurately reproduce spectroscopic signals of Cu zeolites in the literature[6]. To accurately capture the position of d-states and spin transitions present in transition metal exchanged zeolites, spin-orbit coupling was enabled for all calculations. Absorption spectra were calculated by applying a Gaussian broadening of 1000 cm^{-1} to the lowest 100 optical transitions for each image. Static calculations were performed for the A-Cu_2OH dimer described in the literature[7]. The unit cell chosen in our calculations has been described in the literature and as discussed in the past[8], the unit cell volume was set to 830 $Å^3$. Structures for dimers[7], Cu(II)[8] (Cu sites anchored in the 2Al-E Al configuration), CuOH[8], and defect-Cu[6] have been described in the literature.

Important settings for VASP:

General settings: The calculations were performed in a three-step process using the vasp_ncl executable of VASP. All calculations were performed using a hybrid functional with 40% exact exchange (GGA=PE; LHFCALC=.TRUE.; HFSCREEN=0.2; AEXX=0.4), with spin-orbit coupling enabled (LSORBIT=.TRUE.) and a starting magnetic moment of 0 (MAGMOM=#ions*0). Throughout all calculations, an energy cut off of 417 eV was chosen (ENCUT=417). Additionally, GGA_COMPAT=.FALSE. was set. In all calculations we chose gaussian smearing with a sigma value of 0.02 (ISMEAR=0; SIGMA=0.02). In each calculation, the minimum energy spin was enforced accordingly (ISPIN=2, NUPDOWN set to the desired spin).

In the first step, we converged wavefunctions in a single ionic step to energy differences smaller than 10^{-6} (EDIFF=1E-6).
In the second step, we performed a single electronic step (ALGO=EXACT, LOPTICS=.TRUE.; NELM=1) to calculate wavefunctions for a total of 3072 bands (NBANDS=3072).
In the last step, optical spectra were calculated by setting ALGO=TDHF, NOMEGA=50, and OMEGAMAX=15. 101 occupied bands and 200 empty bands were included in the calculation (NBANDSO=101; NBANDSV=200). ENCUTGW was set to 200 and ANTIRES was set to 0.

S1.2: Experimental Methods:

S.1.2.1: Zeolite synthesis:

The SSZ-13 zeolite was synthesized using 6.38 grams of N,N,N Trimethyl ammonium hydroxide solution (25wt% from SACHEM INC) and 1.20 grams (anhydrous after drying) of Zeolite CBV-720 FAU zeolite (from Zeolyst corp., atomic Si/Al ~ 15) as the source of both Si and Al in the synthesis. An additional 4.13 grams of water were added to the Teflon Cup for a Parr 23 ml stainless steel reactor. The reactor was hand-tightened and placed onto a rotating spit (43 RPM) in a Blue M convection oven and heated at 160°C for 6 days while tumbling. The reactor was then recovered, cooled to room temperature, filtered, and washed (to an effluent pH of ~ 9 after a reaction final pH of greater than 12). The washed powder was then examined by X-ray powder diffraction and was found to be the pure phase of SSZ-13 (see Fig. S1 (a)). Furthermore, Scanning Electron Microscopy (SEM) measurements show that the zeolite sample consists of crystallites below 1 µm in diameter. X-Ray measurements were carried out using an XRD diffractometer from Panalytical/Malvern company, Model Empyrean. SEM measurements were performed using a JEOL JSM 6700F.

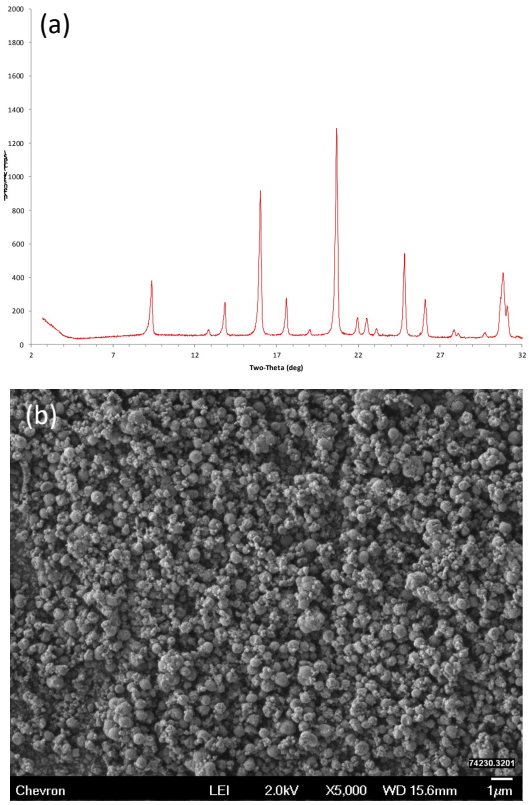

Figure S1: *(a) Diffraction pattern and (b) scanning electron microscopy image of the synthesized zeolite powder. This data confirms the presence of pure phase SSZ-13 with crystallites below 1 µm in diameter.*

The as-made zeolite was then calcined to remove the SDA guest molecule. The calcination consisted of heating in air increasing to a temperature of 1°C/minute to 120°C, which was maintained for 2 hours. Subsequently, heating continued at 1°C/minute to 540°C, which was again maintained for 4 hours before cooling back to room temperature. The calcined material (losing

typically 18% mass) was exposed to two cycles of ion exchange with a 1 molar ammonium nitrate solution at 95°C for 2 hours to ensure that there is no residual Na in the product (the original CBV-720 Faujasite sample contains a very minor amount of residual sodium[9]).

To remove ammonia and generate a protonated zeolite sample for characterization, the material was then treated at 400°C. The micropore volume and surface area was measured using a Micromeritics Tristar 3030. The resulting zeolite sample had a micropore volume of 0.30 cc/gm for nitrogen uptake and a BET calculated surface area of 750 meters squared/gram, which is consistent with typical values for SSZ-13.

S.1.2.2: Ion exchange:
We followed the materials preparation protocol reported by Lobo and coworkers to exchange Cu with SSZ-13[10,11]. Starting with the NH_4-form of SSZ-13, the zeolite was dehydrated at 120 °C (ramp rate of 5 °C/min) for 2h, followed by calcining at 560 °C (ramp rate of 5 °C/min) for 8h in air (80 cm^3/min). The thus obtained H^+-form was cooled to room temperature in air before performing Cu(II) ion-exchange.

We performed Cu(II) ion-exchange using aqueous solutions prepared from copper (II) acetate monohydrate ($Cu(CO_2CH_3)_2 \cdot H_2O$) (Sigma Aldrich, >98% purity). We targeted the Cu/Al ratio for our samples to be between 0.4 and 0.5, close to the theoretical maximum Cu exchange rate for Cu(II) of Cu/Al=0.5. Accordingly, we performed two exchanges sequentially (0.26 g and 0.14 g of $Cu(CO_2CH_3)_2 \cdot H_2O$ in 250 ml and 125 ml water, respectively) with the H^+-form of the SSZ-13 (zeolite mass of 2.51 g). The sample was exchanged at 25 °C for 16 h followed by vacuum drying. To remove the residual acetate after the second exchange cycle, the sample was calcined at 560 °C for 8h in air (80 cm^3/min). Inductively coupled plasma (ICP) analysis performed at Galbraith laboratories for the obtained sample suggested and Si/Al ratio of 14.7 and a Cu/Al ratio of 0.41.

S.1.2.3: UV-vis-NIR measurements:
Diffuse reflectance UV-vis-NIR spectra were recorded after O_2 (Airgas, UHP 99.999% purity) activation for 8h at 450 °C (flowrate and ramp rate of 60 cm^3/min and 5 °C/min, respectively). After the sample was treated under O_2 atmosphere and purged in He (Airgas, UHP 99.999% purity) at room temperature, the sample was transferred to a glovebox (room temperature, H_2O<1ppm and O_2=1ppm) and UV/Vis analyses were performed thereafter. For the measurements, a Maya2000 Pro UV/vis Spectrophotometer (Ocean Optics) equipped with a deuterium/halogen light source (DH-200-BAL from Mikropack) was employed. $BaSO_4$ (99.9%, Sigma-Aldrich) was used as the 100% reflectance standard and as a matrix, with the spectrometer operated in diffuse reflectance mode. Spectra were collected as R% and reported as K-M absorbance after applying the Kubelka-Munk model. We emphasize that - in contrast to transmission - the applied Kubelka-Munk correction might influence relative spectral intensities[12].

S2: Importance of Molecular Dynamics and Spin Orbit Coupling for Calculating Optical Spectra

In the past, the importance of sampling multiple structural snapshots from molecular dynamics calculations to obtain accurate spectra has been pointed out[4,6]. However, the impact of the inclusion of spin orbit coupling (SOC) is still poorly understood. In order to compare the different levels of theory, we study spectra for the A-Cu_2OH site either from static calculations or as average over multiple structural snapshots. Additionally, we compare the obtained spectra with and without SOC included. Results are shown in Figure S2. These results show significant differences for calculations at different levels of theory.

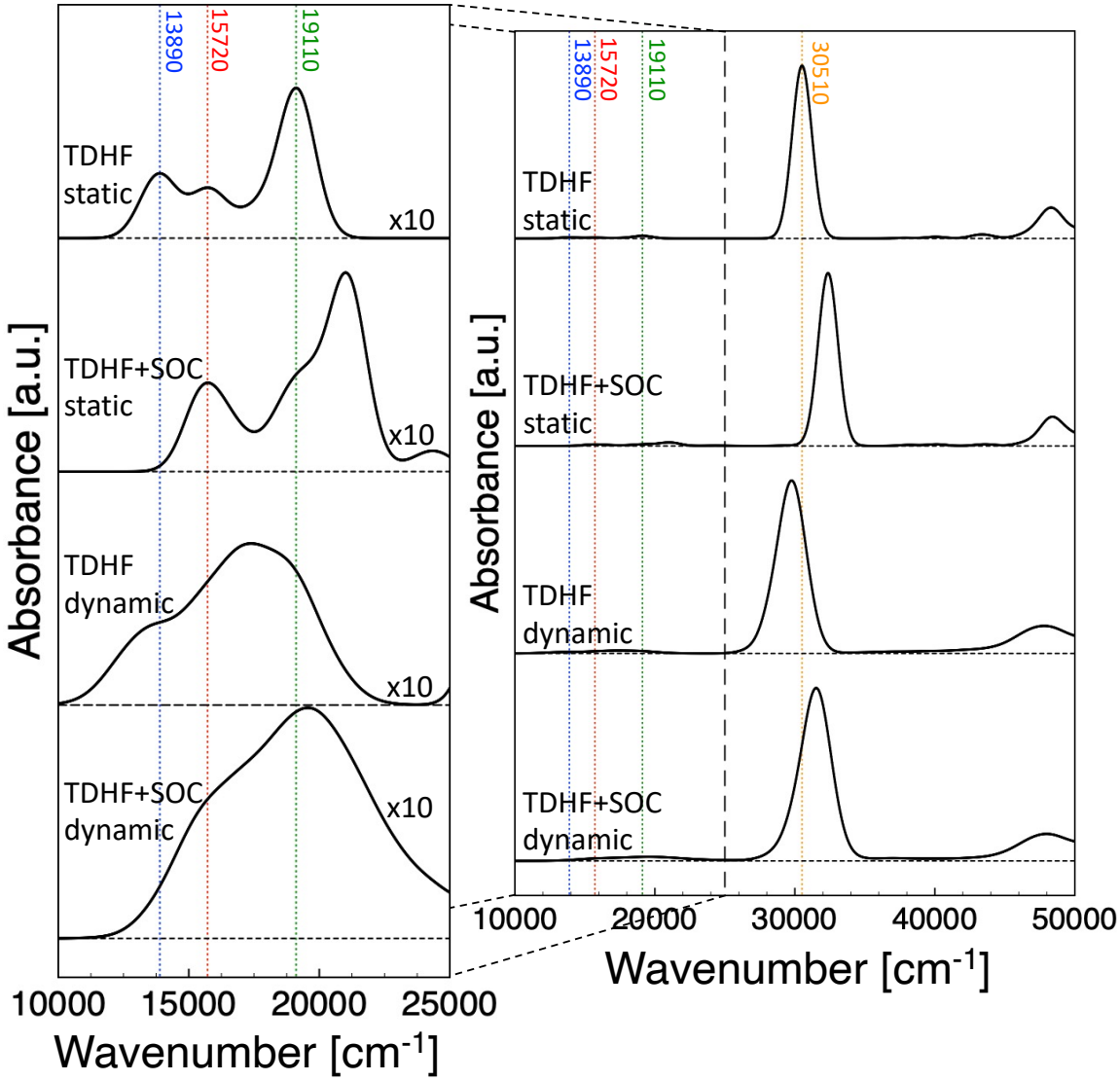

Figure S2: *Theoretically predicted optical spectra for A-Cu_2OH at different levels of theory between 10000 cm^{-1} and 25000 cm^{-1} (left panel), and 10000 cm^{-1} and 50000 cm^{-1} (right) . Spectra are shown as solid black lines and the zero-intensity line for each spectrum is shown as horizontal dashed black line. Peaks for the statically calculated TDHF spectrum are marked with dashed, vertical lines in various colors for readability. For better visibility, spectra in the left panel have been multiplied by the factor indicated in the legend. Both, the inclusion of spin orbit coupling (TDHF+SOC) and the calculation of spectra using*

molecular dynamics simulations (dynamic) significantly alter the obtained spectra compared to TDHF calculations for structures optimized at 0K (TDHF static).

The large shifts in peak positions and intensities upon the inclusion of SOC is surprising. There are two potential explanations for the observed differences, namely (i) SOC leads to significant differences in the relative energetics between the different orbitals, or (ii) singlet-triplet transitions, which are correctly captured by SOC, are the cause of the differences in the calculated spectra. In order to understand the mechanisms leading to the shifts in spectroscopic signals, we compare the DOS calculated without and with the inclusion of spin-orbit coupling (see Fig. S3). We find that the DOS is almost identical in both cases, which indicates that most likely singlet-triplet transitions are responsible for the shifts in the predicted spectra. Even though singlet-triplet transitions are often assumed to be weak, intense singlet-triplet transitions have been observed in the photoluminescence of Ag clusters in zeolites, which is typically attributed to singlet triplet transitions[13,14]. Similarly, strong photoluminescence signals have been observed for Cu monomers in SSZ-13[6]. Hence, strong singlet-triplet transitions for Cu sites in zeolites are expected.

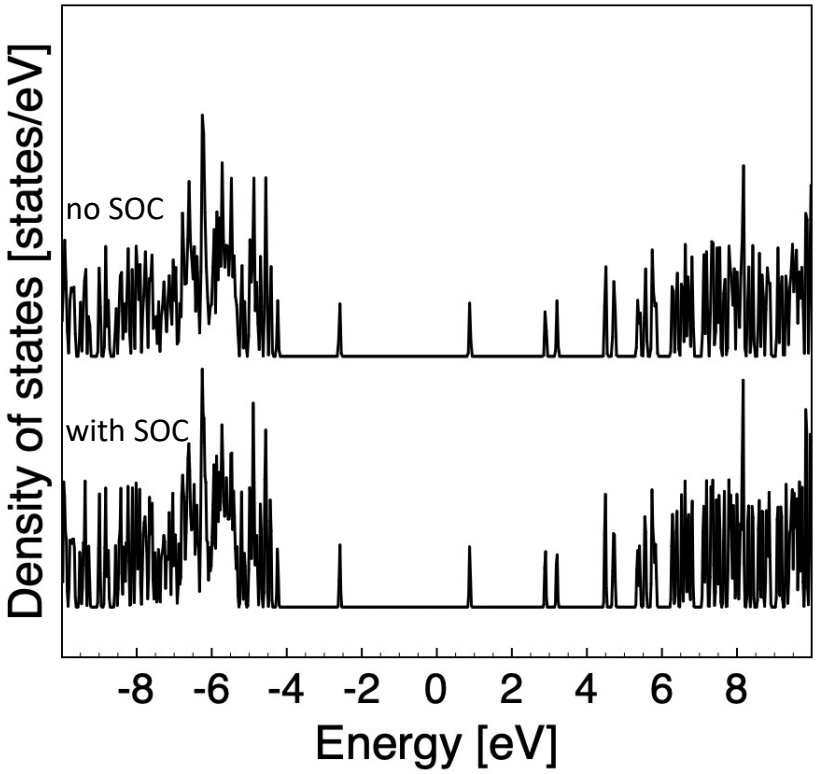

Figure S3: *Comparison of the DOS calculated at HSE06(0.4 EXX) level of theory without (no SOC) and with spin orbit coupling (SOC). The DOS is displayed as black lines and the energy is given in eV. For easier comparison, the DOS calculated without SOC is displayed as sum of spin-up and spin-down components.*

So far, we have shown the impact of SOC on the spectrum of one site, namely A-Cu_2OH. However, it is not clear whether similar trends are observed for spectra of other sites as well. We therefore focus on static calculations of the most stable hydroxylated dimers (A-$Cu_2O_2H_2$, B-$Cu_2O_2H_2$, C-Cu_2OH, D-Cu_2OH) as well as one Cu monomer (CuOH) and compare spectra calculated with and without SOC. Results are shown in Fig. S4. In particular for the dimers, we see a similar change in spectra upon the inclusion of SOC. We hypothesize that the strong singlet-triplet transitions are

associated with the covalent Cu-O bond found in these structures. This hypothesis is in agreement with observations for photoluminescence spectra of Cu(I) sites in SSZ-13[6]. Here, Cu(I) bonded at framework defects showed significantly stronger singlet-triplet transitions than extraframework Cu(I), where the bond between Cu and framework O has a more covalent character. For CuOH, we also see the appearance of singlet triplet transitions. However, they are significantly weaker than for the dimers and might not be observed in experimental measurements.

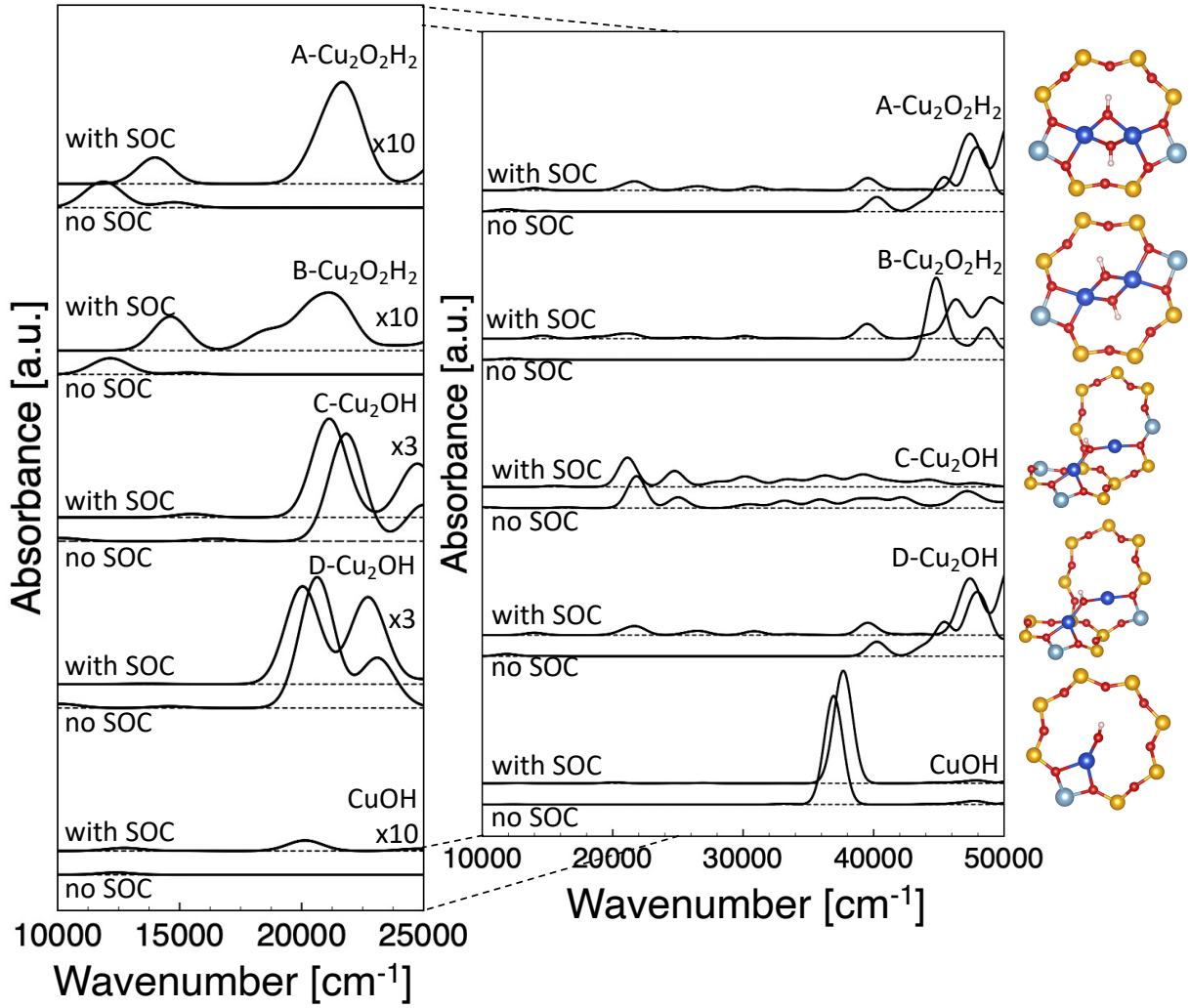

Figure S4: *Comparison between theoretically predicted optical spectra with or without SOC for optimized structures of A-$Cu_2O_2H_2$, B-$Cu_2O_2H_2$, C-Cu_2OH, D-Cu_2OH, and CuOH between 10000 cm^{-1} and 25000 cm^{-1} (left panel) and 10000 cm^{-1} and 50000 cm^{-1}(right) . Spectra are shown as solid black lines and the zero-intensity line for each spectrum is shown as horizontal dashed black line. For better visibility, spectra in the left panel have been multiplied by the factor indicated in the legend. Colors in atomistic pictures on the right correspond to Figure 1 in the main text.*

S3: Calculated Spectra for various Cu sites:

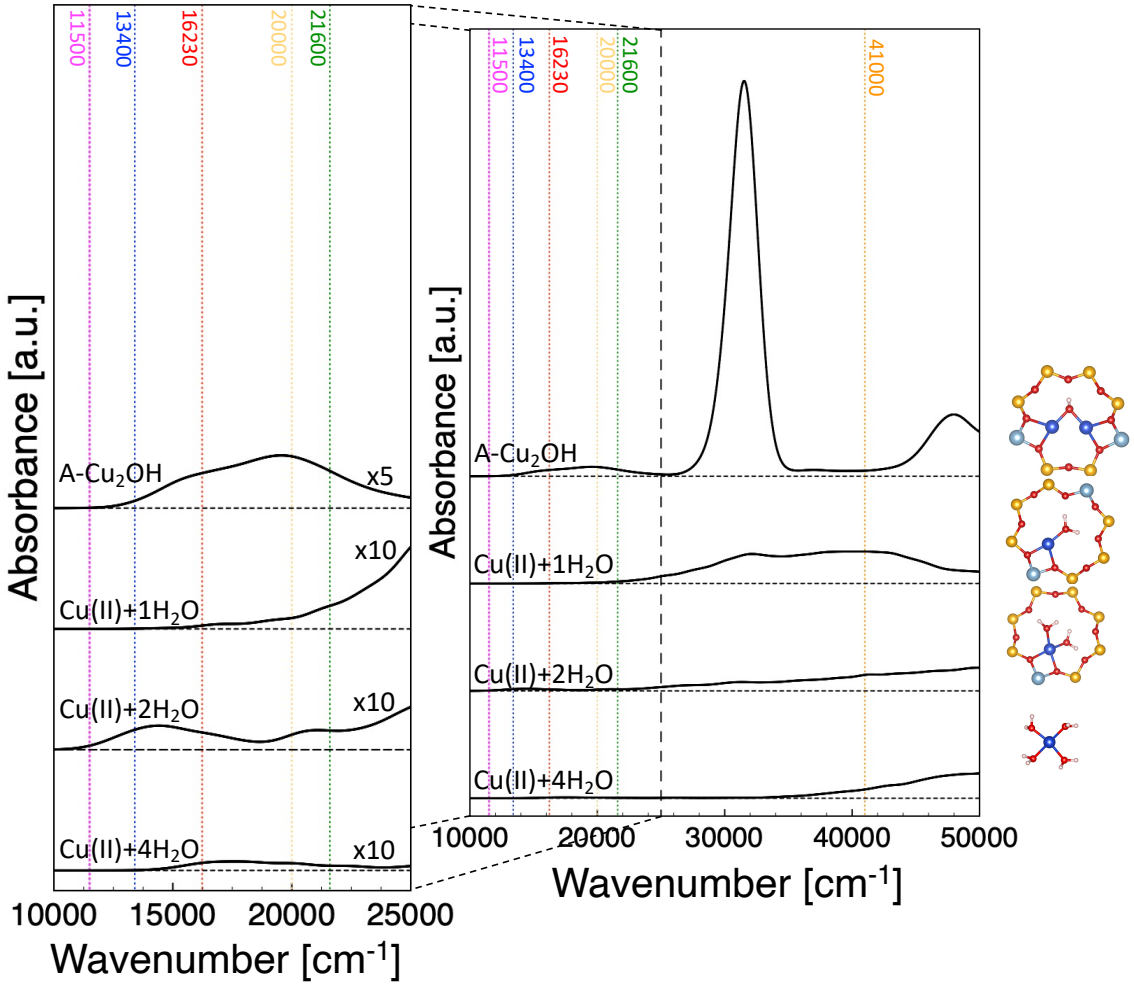

Figure S5: *Theoretically predicted optical spectra for A-Cu_2OH, Cu(II)+1H_2O, Cu(II)+2H_2O, and Cu(II)+4H_2O between 10000 cm^{-1} and 25000 cm^{-1} (left panel) and 10000 cm^{-1} and 50000 cm^{-1}(right) . Spectra are shown as solid black lines and the zero-intensity line for each spectrum is shown as horizontal dashed black line. Experimentally observed peaks and shoulders are marked with dashed, vertical lines in various colors for readability. For better visibility, spectra in the left panel have been multiplied by the factor indicated in the legend. Colors in atomistic pictures on the right correspond to Figure 1 in the main text.*

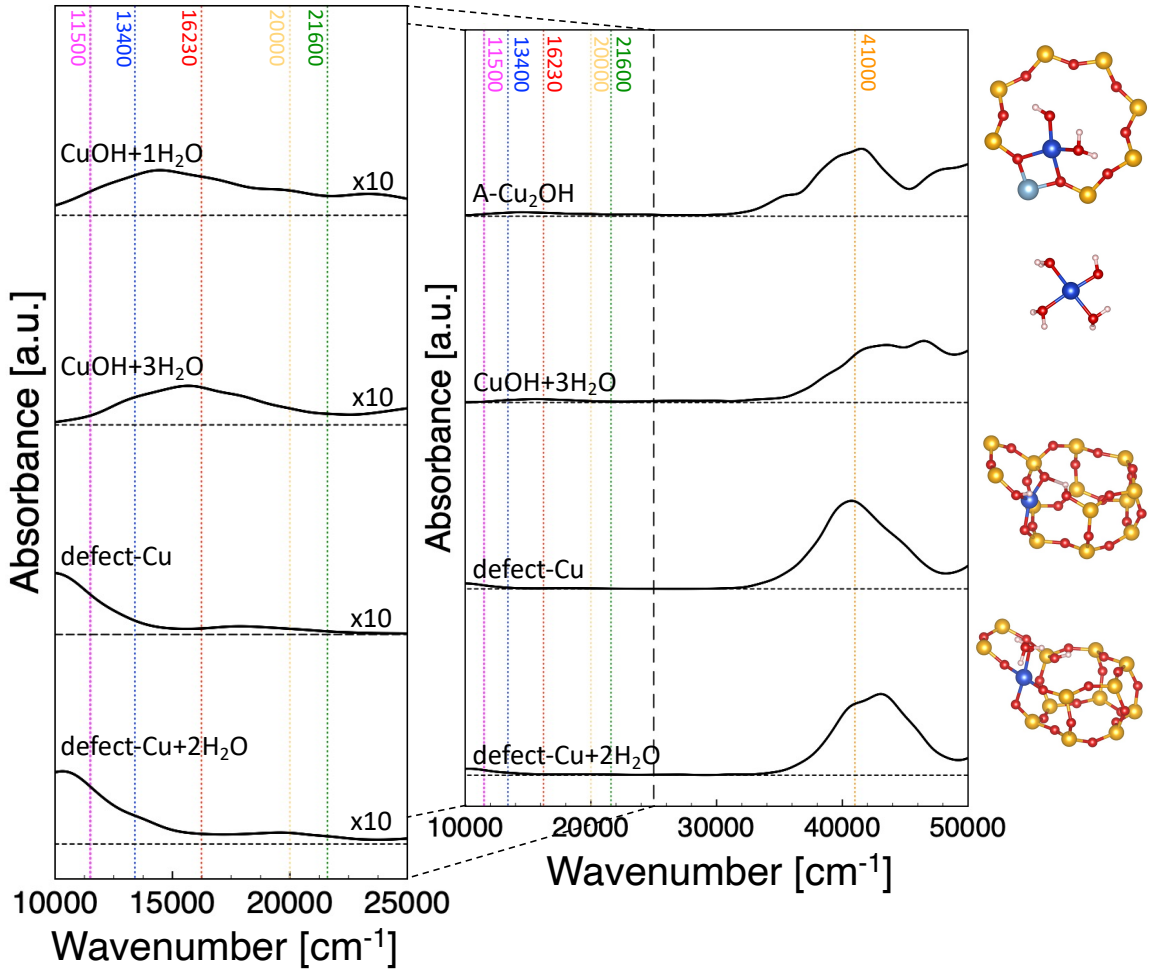

Figure S6: *Theoretically predicted optical spectra for $CuOH+1H_2O$, $CuOH+3H_2O$, defect-Cu, and defect-Cu+$2H_2O$ between 10000 cm^{-1} and 25000 cm^{-1} (left panel) and 10000 cm^{-1} and 50000 cm^{-1}(right) . Spectra are shown as solid black lines and the zero-intensity line for each spectrum is shown as horizontal dashed black line. Experimentally observed peaks and shoulders are marked with dashed, vertical lines in various colors for readability. For better visibility, spectra in the left panel have been multiplied by the factor indicated in the legend. Colors in atomistic pictures on the right correspond to Figure 1 in the main text.*

S4: Calculated Spectra for various Cu-oxo dimers:

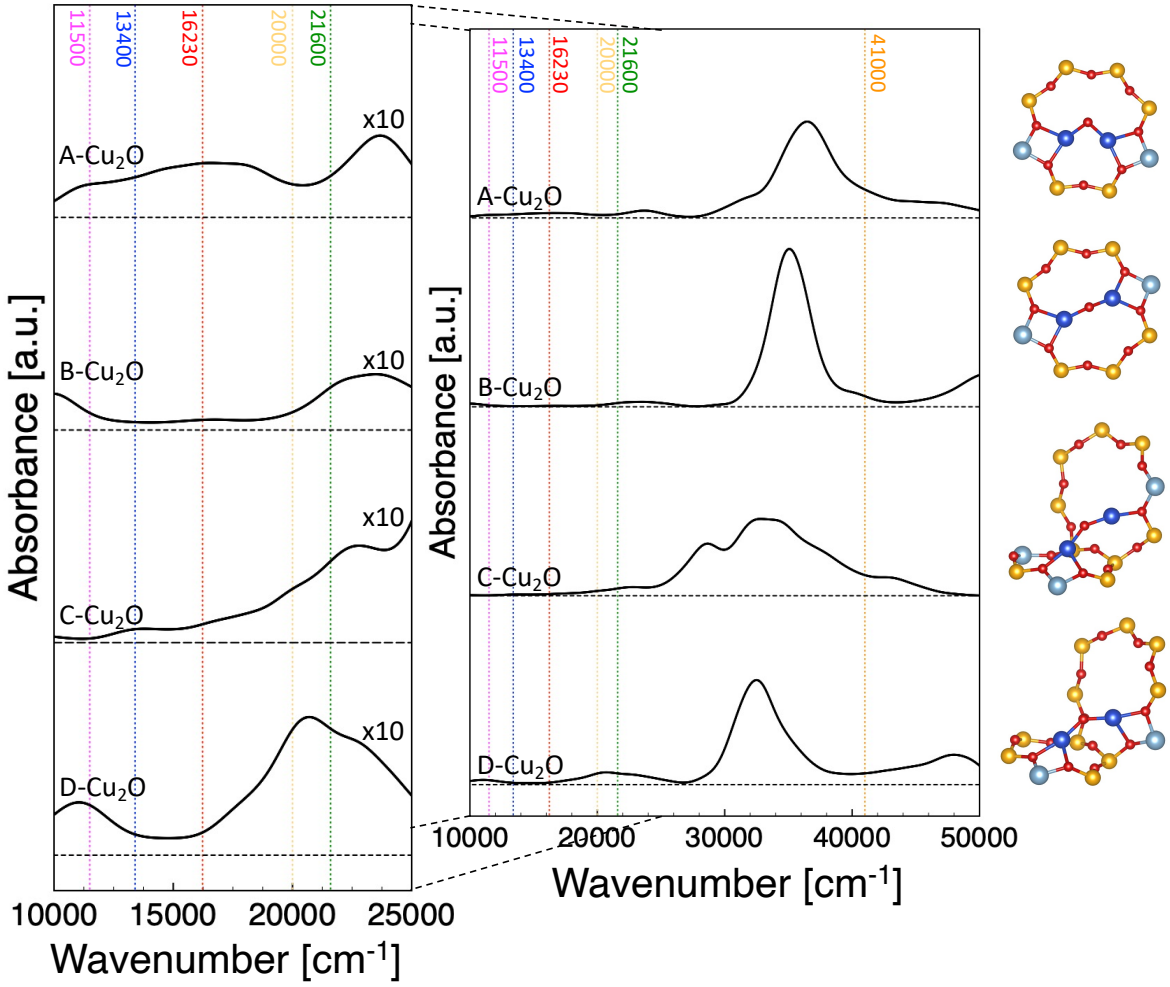

Figure S7: *Theoretically predicted optical spectra for A-Cu_2O, B-Cu_2O, C-Cu_2O, and D-Cu_2O between 10000 cm^{-1} and 25000 cm^{-1} (left panel) and 10000 cm^{-1} and 50000 cm^{-1}(right) . Spectra are shown as solid black lines and the zero-intensity line for each spectrum is shown as horizontal dashed black line. Experimentally observed peaks and shoulders are marked with dashed, vertical lines in various colors for readability. For better visibility, spectra in the left panel have been multiplied by the factor indicated in the legend. Colors in atomistic pictures on the right correspond to Figure 1 in the main text.*

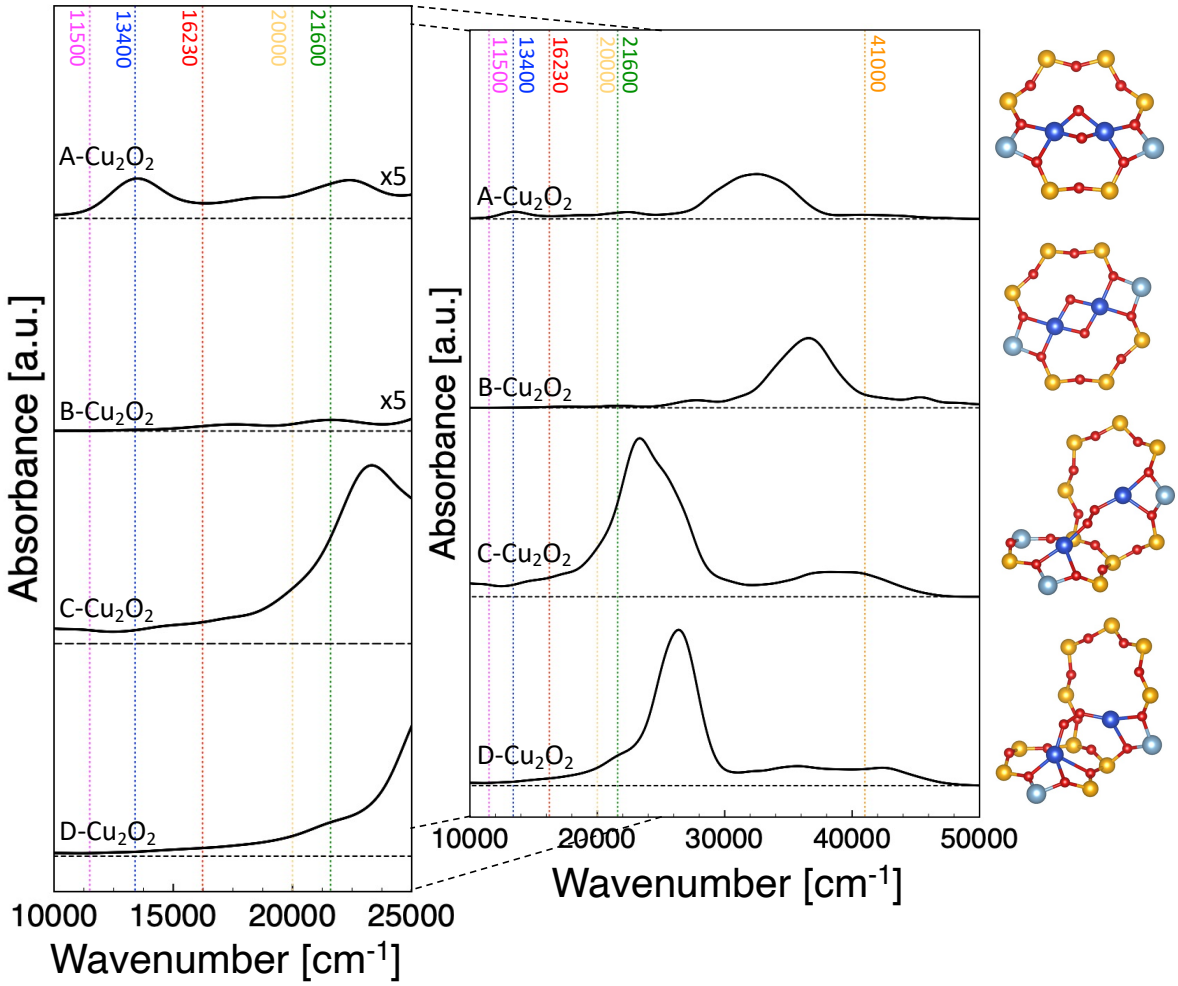

Figure S8: *Theoretically predicted optical spectra for A-Cu_2O_2, B-Cu_2O_2, C-Cu_2O_2, and D-Cu_2O_2 between 10000 cm^{-1} and 25000 cm^{-1} (left panel) and 10000 cm^{-1} and 50000 cm^{-1} (right) . Spectra are shown as solid black lines and the zero-intensity line for each spectrum is shown as horizontal dashed black line. Experimentally observed peaks and shoulders are marked with dashed, vertical lines in various colors for readability. For better visibility, spectra in the left panel have been multiplied by the factor indicated in the legend. Colors in atomistic pictures on the right correspond to Figure 1 in the main text.*

References:

(1) Kresse, G.; Furthmüller, J. Efficiency of Ab-Initio Total Energy Calculations for Metals and Semiconductors Using a Plane-Wave Basis Set. *Comput. Mater. Sci.* **1996**, *6* (1), 15–50.

(2) Kresse, G.; Joubert, D. From Ultrasoft Pseudopotentials to the Projector Augmented-Wave Method. *Phys. Rev. B* **1999**, *59* (3), 1758–1775.

(3) Blöchl, P. E. Projector Augmented-Wave Method. *Phys. Rev. B* **1994**, *50* (24), 17953–17979.

(4) Li, H.; Paolucci, C.; Khurana, I.; Wilcox, L. N.; Göltl, F.; Albarracin-Caballero, J. D.; Shih, A. J.; Ribeiro, F. H.; Gounder, R.; Schneider, W. F. Consequences of Exchange-Site Heterogeneity and Dynamics on the UV-Visible Spectrum Of. *Chem. Sci.* **2019**, *10*, 2373–2384.

(5) Casida, M. E. Generalization of the Optimized-Effective-Potential Model to Include Electron Correlation: A Variational Derivation of the Sham-Schlüter Equation for the Exact Exchange-Correlation Potential. *Phys. Rev. A* **1995**, *51* (3), 2005–2013.

(6) Göltl, F.; Conrad, S.; Wolf, P.; Müller, P.; Love, A. M.; Burt, S. P.; Wheeler, J. N.; Hamers, R. J.; Hummer, K.; Kresse, G.; et al. UV–Vis and Photoluminescence Spectroscopy to Understand the Coordination of Cu Cations in the Zeolite SSZ-13. *Chem. Mater.* **2019**, *31*, 9582–9592.

(7) Göltl, F.; Bhandari, S.; Mavrikakis, M. Thermodynamics Perspective on the Stepwise Conversion of Methane to Methanol over Cu-Exchanged SSZ-13. *ACS Catal.* **2021**, *11*, 7719–7734.

(8) Göltl, F.; Love, A. M.; Hermans, I. Developing a Thermodynamic Model for the Interactions Between Water and Cu in the Zeolite SSZ-13. *J. Phys. Chem. C* **2017**, *121*, 6160–6169.

(9) Zones, S. I.; Lew, C. M.; Xie, D.; Davis, T. M.; Schmidt, J. E.; Saxton, R. J. Studies on the Use of Faujasite as a Reagent to Deliver Silica and Alumina in Building New Zeolite Structures with Organo-Cations. *Microporous Mesoporous Mater.* **2020**, *300* (March), 110162.

(10) Ipek, B.; Lobo, R. F. Catalytic Conversion of Methane to Methanol on Cu-SSZ-13 Using N_2O as Oxidant. *Chem. Commun.* **2016**, *5* (300), 1668–1686.

(11) Ipek, B.; Wulfers, M. J.; Kim, H.; Göltl, F.; Hermans, I.; Smith, J. P.; Booksh, K. S.; Brown, C. M.; Lobo, R. F. Formation of $[Cu_2O_2]^{2+}$ and $[Cu_2O]^{2+}$ toward C-H Bond Activation in Cu-SSZ-13 and Cu-SSZ-39. *ACS Catal.* **2017**, *7* (7), 4291–4303.

(12) Negri, C.; Signorile, M.; Porcaro, N. G.; Borfecchia, E.; Berlier, G.; Janssens, T. V. W.; Bordiga, S. Dynamic CuII/CuI Speciation in Cu-CHA Catalysts by in Situ Diffuse Reflectance UV–Vis-NIR Spectroscopy. *Appl. Catal. A Gen.* **2019**, *578*, 1–9.

(13) Fenwick, O.; Coutiño-Gonzalez, E.; Grandjean, D.; Baekelant, W.; Richard, F.; Bonacchi, S.; De Vos, D.; Lievens, P.; Roeffaers, M.; Hofkens, J.; et al. Tuning the Energetics and Tailoring the Optical Properties of Silver Clusters Confined in Zeolites. *Nat. Mater.* **2016**, *15* (June), 1–11.

(14) Grandjean, D.; Coutiño-Gonzalez, E.; Cuong, N. T.; Fron, E.; Baekelant, W.; Aghakhani, S.; Schlexer, P.; D'acapito, F.; Banerjee, D.; Roeffaers, M. B. J.; et al. Origin of the Bright Photoluminescence of Few-Atom Silver Clusters Confined in LTA Zeolites. *Science (80-.).* **2018**, *361* (6403), 686–690.